Mon. Not. R. Astron. Soc. **333,** 133–144 (2002)

The 2dF Galaxy Redshift Survey: galaxy luminosity functions per spectral type

Darren S. Madgwick,[1★] Ofer Lahav,[1] Ivan K. Baldry,[2] Carlton M. Baugh,[3] Joss Bland-Hawthorn,[4] Terry Bridges,[4] Russell Cannon,[4] Shaun Cole,[3] Matthew Colless,[5] Chris Collins,[6] Warrick Couch,[7] Gavin Dalton,[8] Roberto De Propris,[7] Simon P. Driver,[9] George Efstathiou,[1] Richard S. Ellis,[10] Carlos S. Frenk,[3] Karl Glazebrook,[2] Carole Jackson,[5] Ian Lewis,[4] Stuart Lumsden,[11] Steve Maddox,[12] Peder Norberg,[3] John A. Peacock,[13] Bruce A. Peterson,[5] Will Sutherland[13] and Keith Taylor[10]

[1]*Institute of Astronomy, University of Cambridge, Madingley Road, Cambridge CB3 0HA*
[2]*Department of Physics and Astronomy, Johns Hopkins University, Baltimore, MD 21218-2686, USA*
[3]*Department of Physics, South Road, Durham DH1 3LE*
[4]*Anglo-Australian Observatory, PO Box 296, Epping, NSW 2121, Australia*
[5]*Research School of Astronomy and Astrophysics, The Australian National University, Weston Creek, ACT 2611, Australia*
[6]*Astrophysics Research Institute, Liverpool John Moores University, Twelve Quays House, Birkenhead L14 1LD*
[7]*Department of Astrophysics, University of New South Wales, Sydney, NSW 2052, Australia*
[8]*Department of Physics, Keble Road, Oxford OX1 3RH*
[9]*School of Physics and Astronomy, North Haugh, St Andrews, Fife KY6 9SS*
[10]*Department of Astronomy, Caltech, Pasadena, CA 91125, USA*
[11]*Department of Physics, University of Leeds, Woodhouse Lane, Leeds LS2 9JT*
[12]*School of Physics and Astronomy, University of Nottingham, Nottingham NG7 2RD*
[13]*Institute for Astronomy, University of Edinburgh, Royal Observatory, Blackford Hill, Edinburgh EH9 3HJ*

Accepted 2002 January 31. Received 2001 December 11; in original form 2001 July 13

ABSTRACT

We calculate the optical b_J luminosity function (LF) of the 2dF Galaxy Redshift Survey (2dFGRS) for different subsets defined by their spectral properties. These spectrally selected subsets are defined using a new parameter, η, which is a linear combination of the first two projections derived from a Principal Component Analysis. This parameter η identifies the average emission- and absorption-line strength in the galaxy rest frame spectrum, and hence is a useful indicator of the present star formation. We use a total of 75 000 galaxies in our calculations, chosen from a sample of high signal-to-noise ratio, low-redshift galaxies observed before 2001 January. We find that there is a systematic steepening of the faint-end slope (α) as one moves from passive ($\alpha = -0.54$) to active ($\alpha = -1.50$) star-forming galaxies, and that there is also a corresponding faintening of the rest frame characteristic magnitude $M^* - 5\log_{10}(h)$ (from -19.6 to -19.2). We also show that the Schechter function provides a poor fit to the quiescent (Type 1) LF for very faint galaxies [$M_{b_J} - 5\log_{10}(h)$ fainter than -16.0], perhaps suggesting the presence of a significant dwarf population. The LFs presented here give a precise confirmation of the trends seen previously in a much smaller preliminary 2dFGRS sample, and in other surveys. We also present a new procedure for determining self-consistent *k*-corrections, and investigate possible fibre-aperture biases.

Key words: galaxies: distances and redshifts – galaxies: elliptical and lenticular, cD – galaxies: evolution – galaxies: formation – galaxies: stellar content.

★E-mail: dsm@ast.cam.ac.uk

1 INTRODUCTION

It is well established that the measurement of the galaxy luminosity function (LF) is sensitive to the type of galaxy being sampled. Morphologically, early-type galaxies tend to be systematically brighter than their late-type counterparts, resulting in LF estimates with significantly brighter M^* and shallower faint-end slope α (e.g. Efstathiou, Ellis & Peterson 1988, hereafter EEP98; Loveday et al. 1992; Blanton et al. 2001). Similar trends are also present if one selects galaxies based on Hα equivalent widths (Loveday, Tresse & Maddox 1999), [O II] equivalent widths (Ellis et al. 1996) or colour (Lin et al. 1996; Marzke & Da Costa 1997). Understanding and being able to quantify this variation in the LF is of great importance to a full understanding of galaxy formation and evolution.

Up until now the greatest obstacle faced when attempting to determine how the LF varied with different galaxy properties was the fact that one was required to divide already small data sets, thereby losing much of the statistical significance in the LF estimations. In this paper we address this issue by making use of a subset of the galaxies observed to date in the 2dF Galaxy Redshift Survey (2dFGRS; Colless et al. 2001). This subset is the largest single data set used in the calculation of LFs, and can easily be divided several times whilst still maintaining very precise statistics.

The 2dFGRS is a joint UK-Australian effort to map the distribution of galaxies down to an extinction corrected b_J magnitude of 19.45 (median redshift $z \simeq 0.1$). In so doing, we expect to obtain 250 000 galaxy spectra from which redshifts can be determined. This is a factor of 10 more than any previous redshift survey.

In order to divide our data set in a meaningful way, we develop in this paper a classification of the galaxies based upon their observed spectra. As with other astronomical data, there are different approaches for analysing galaxy spectra (see, e.g., Lahav 2000, and references therein). If one has a well-defined physical model for galaxy spectra, then it is appropriate to estimate parameters of interest (such as age and star formation rate), e.g. by maximum likelihood, directly using all the spectral bins, or via a compressed version of the data designed to give maximum information on the physical parameters of interest (e.g. Heavens, Jimenez & Lahav 2000). If, on the other hand, one prefers to let the data 'speak for themselves' in a model-independent way, then it is more useful to look at the distribution of the galaxies in the high-dimensional space defined by the spectral bins. It is then possible to look either for distinct groups, e.g. early and late types, or more refined classes (e.g. Slonim et al. 2001). An alternative, which we present here, is to find a continuous (sequence-like) parametrization of the spectral features, which can later be divided into subsets. The parametrization we develop is denoted by η, and essentially represents a measure of the average absorption- or emission-line strength present in each galaxy's spectrum. This classification is robust to the known instrumental uncertainties, and also has the advantage of being easily interpreted in terms of the current star formation present in each galaxy.

The set of galaxies we use in this paper comprises a sample of 75 000 galaxy spectra. This is more than 12 times larger than the one used in our previous analysis (Folkes et al. 1999, hereafter F99) and is by far the largest sample used to date.

As well as showing the latest LF determinations, we will also present a new procedure for calculating self-consistent k-corrections and investigate possible fibre-aperture biases.

The outline of this paper is as follows. Section 2 briefly summarizes the 2dFGRS and describes the data set we are using, Section 3 outlines our method for dividing the data set based on our parametrization of the galaxy spectral type, η. Section 4 gives a detailed description of the calculations involved in estimating the LF, and in Section 5 we discuss our results and future work.

2 THE 2DFGRS DATA

The 2dFGRS has already observed approximately 200 000 unique galaxies for which it has obtained redshifts. The survey, once complete, will cover approximately 2000 deg^2 on the sky, split between two independent strips: one in the northern Galactic hemisphere and the other centred roughly on the South Galactic Pole (SGP). In addition to this, there are 99 random fields in the southern Galactic cap.

The 2dF instrument itself is capable of observing up to 400 galaxy spectra simultaneously (Lewis et al. 2001). Each galaxy has been selected from a revised and extended version of the Automated Plate Measuring (APM) galaxy catalogue (Maddox, Efstathiou & Sutherland 1990) in order to determine its position and magnitude. It is then observed as part of the survey through a 140-μm ($\sim$2 arcsec) diameter optical fibre. The b_J magnitudes we use in this analysis are total magnitudes derived from updated versions of the original APM scans. These magnitudes have been updated to take into account new CCD calibration data (see Colless et al. 2001 and Norberg et al. 2001), and are believed to have an rms error of approximately ± 0.15 mag.

Each of the spectra observed using the 2dF instrument spans 1024 channels with a spectral scale of 4.3 Å per pixel; the FWHM is measured by arc lines to be of the order of 1.8–2.5 pixels. Typically, at the survey limit the observed spectra have an average signal-to-noise ratio of $\sim$10 per pixel, sufficient for determining redshifts and performing spectral analyses. For the purposes of our spectral analysis we have restricted ourselves to the redshift range of $0.01 < z < 0.2$, so that we are left with a uniform sample of galaxy spectra in the rest frame wavelength range spanning [O II] to Hα. A detailed outline of the spectral reduction pipeline is given in F99 and Colless et al. (2001), which we follow with only minor modifications.

The data that we have available for this analysis include all observations up until 2001 January. At this stage a total of 111 404 and 60 062 galaxy spectra had been obtained in the SGP and NGP regions respectively. From these objects we remove those which did not receive accurate redshifts ($Q < 3$; Colless et al. 2001), repeated observations and spectra with particularly low signal-to-noise ratio (≤ 10). This leaves us with 78 994 (SGP) and 44 937 (NGP) galaxies for use in our spectral analysis. Because of interference from sky emission and atmospheric absorption, we have made a further restriction to our redshift range such that $z \leq 0.15$. This cut ensures that the Hα line in our spectra is not corrupted. Note that this is a problem only for the small redshift range $0.15 < z < 0.17$; however, we have also excluded the galaxies with $z > 0.17$ in order to simplify our analysis. Imposing this cut and removing spectra observed in poor-quality fields (Section 4.1) leaves us with 43 449 (SGP) and 32 140 (NGP) galaxies. A total of 75 589 unique galaxies will therefore be used in our subsequent analysis and measurement of the LF.

3 SPECTRAL TYPES

The spectral classification presented here is based upon a Principal Component Analysis (PCA) of the galaxy spectra. PCA is a

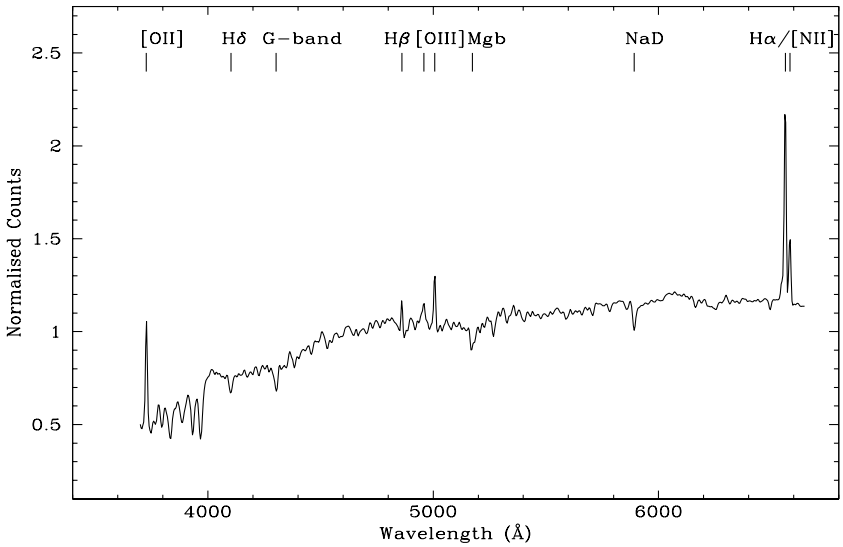

Figure 1. The average spectrum of the $M_{b_J} - 5\log_{10}(h) > -18$ volume-limited sample of galaxies. The main spectral features present are labelled.

statistical technique which has been used with considerable success by multiple authors in the past (e.g. Connolly et al. 1995; Folkes, Lahav & Maddox 1996; Bromley et al. 1998; Glazebrook, Offer & Deeley 1998; F99) to deal with large multidimensional data sets. A detailed mathematical formulation of the PCA adopted here in is given in F99. Note that the most significant difference between this formulation and that used by other authors (e.g. Connolly et al. 1995) is that our spectra have been mean-subtracted (Fig. 1) before constructing the covariance matrix. This makes no substantial difference to the analysis, since using other methods simply yields the mean spectrum as the first component.

We note that throughout the remainder of this paper we will denote the eigenvectors (herein eigenspectra) as $\boldsymbol{PC}_1$, $\boldsymbol{PC}_2$, etc. and the projections on to these axes by pc_1, pc_2, etc.

3.1 Applying PCA

PCA is a useful technique in that it allows us to easily visualize a multidimensional population in terms of just a handful of significant components. It does this by identifying the components of the data (in this case the galaxy spectra) which are the most discriminatory between each galaxy. The significance of each component is measured in terms of its contribution to the variance over the sample, and is determined in the PCA. This allows us to identify just the most significant components for future use. It is clear from such a formalism that any clustering in a space defined by the PCA is indicative of distinct subpopulations within the sample.

In terms of reduced dimensionality we find, after applying the PCA to our galaxy spectra, that rather than using the original 738 spectral channels to describe each spectrum, we can use only two projections and still retain two-thirds of the total variance within the population. Indeed, we can retain 50 per cent of the total variance just from the first component (the total variance of the population includes noise, and hence this is an underestimate of the true fraction of variance in these projections). The significance of each successive principal component drops off very sharply, so these first few components are by far the most important (Table 1).

Admittedly it is not clear a priori whether retaining maximum variance over the spectral population also retains a corresponding maximum of physical information regarding each galaxy. However, in this paper, and also in previous independent analyses, it is found empirically that the components dominating the spectral distribution do in fact relate well to physical attributes For example, morphology and other well-known diagnostics such as the continuum slope (colour), the average emission/absorption line strength and the strength of the Hα line (see, e.g., Ronen, Aragón-Salamanca & Lahav 1999).

Table 1. The relative importance (measured as variance) of the first eight principal components.

Component	Variance (%)	Component	Variance (%)
1	51	5	1.7
2	15	6	1.3
3	3.4	7	0.99
4	2.4	8	0.84

It is worth noting here that there are several limitations to using PCA which the reader should bear in mind. The most important of these is that it imposes linearity on the data set. This is certainly not a satisfactory approximation in all cases, but the general ability of the analysis to reconstruct galaxy spectra successfully with only the first few projections suggests that such an approximation is valid. We also note that in this analysis (as in previous work) we have restricted ourselves to deriving only the most general classification scheme. In so doing, we ignore several distinct subpopulations in our data set such as starbursts and AGNs. In fact, it should be possible to take another approach, and to target the analysis on finding these subpopulations.

3.2 Volume-limited PCA

Due to the large number of galaxy spectra acquired so far in the 2dFGRS it has now become possible to consider volume-limited subsets of the galaxies for use in the PCA. This approach is much more optimal compared to considering the entire flux-limited data set in which the spectral population can be biased by relationships between the luminosity and type of galaxies.

We find that using an absolute $M_{b_J} - 5\log_{10}(h)$ magnitude limit of -18.0 (corresponding to a redshift of $z \simeq 0.1$) gives a

representative subset of the local population whilst still retaining 35 289 galaxies in the analysis, a very large fraction of the total. We have therefore chosen to perform the PCA on this subset of the population in order to determine the principal components. It is then a trivial matter to use these components to derive the individual projections for each of the remaining galaxies outside of our volume-limited sample. The average spectrum of this volume-limited sample is shown in Fig. 1, and the projections in the plane defined by the first two principal components are shown in Fig. 2.

3.3 Interpreting the PCA

We can identify general trends in the distribution of projections shown in Fig. 2 by considering the physical significance of the first two eigenspectra. We find that whilst the first eigenspectrum contains an approximately equal contribution from both the continuum and the emission/absorption line strengths, the second is dominated by the latter. Therefore by taking certain linear combinations of the two, we can either maximize or minimize the contribution from the line features in the spectrum (Fig. 3). Such a transformation of axes allows us to easily interpret the distribution in Fig. 2 as both a sequence in colour from red (bottom left) to blue (top right) and an orthogonal sequence from absorption (top left) to emission (bottom right).

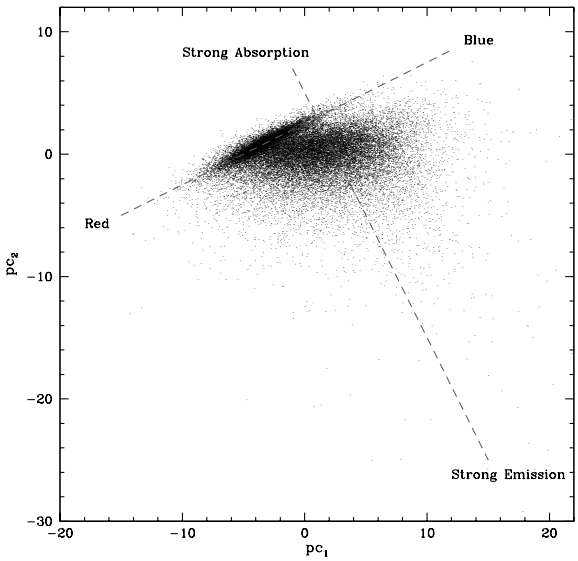

Figure 2. Projections (pc_1 and pc_2) in the space defined by the first two eigenspectra derived from the PCA for the $M_{b_j} - 5\log_{10}(h) < -18$ sample of galaxy spectra. The trends illustrated have been derived from the eigenspectra by identifying the linear combinations that either maximize the influence of the absorption/emission features or minimize them.

3.4 Instrumental effects

The 2dF instrument was designed to measure large numbers of redshifts in as short an observing time as possible. In so doing, it has made very large projects such as the 2dFGRS possible. However, in order to optimize the number of redshifts that can be measured in a given period of time, compromises have had to be made with respect to the spectral quality of the observations. Therefore, if one wishes to characterize the observed galaxy population in terms of their spectral properties, care must be taken to ensure that these properties are robust to the instrumental uncertainties (see, e.g., Lewis et al. 2001 for a more detailed discussion).

The 2dF instrument makes use of up to 400 optical fibres with a diameter of 140 μm (corresponding to 2.0–2.16 arcsec on the sky, depending on plate position). The quality and representativeness of the observed spectra can be compromised in many ways, the most significant of which are as follows.

(1) Astrometric errors in determining the actual position of the galaxy on the sky can result in the fibre being placed in a position that is not optimal for light collection. In general, the position of a galaxy centre is known to within 0.4 arcsec.

(2) Given a known galaxy location on the sky, the robotic positioner will place the fibre to within 20 μm. The rms error in placing this fibre is found to be 11 μm (0.16 arcsec).

(3) The observed colour (continuum slope) of the galaxy

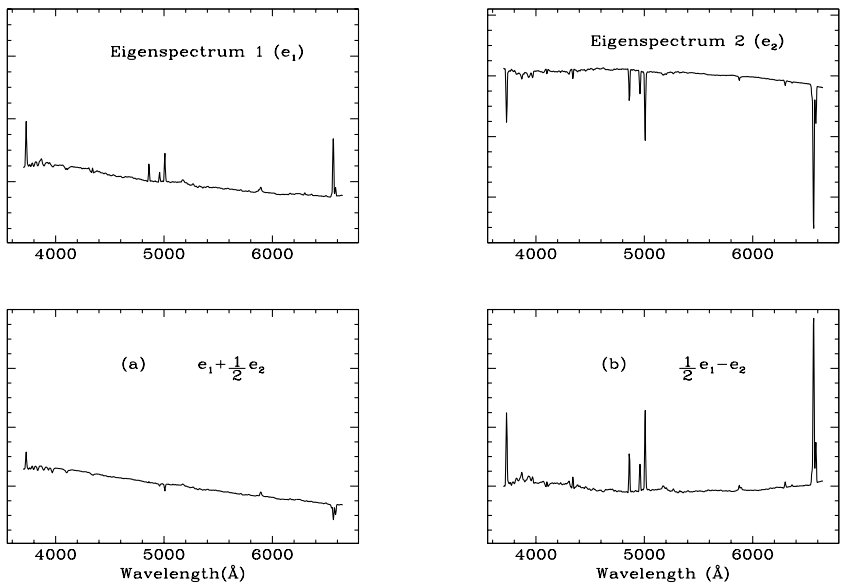

Figure 3. The first two eigenspectra are shown in the top two panels, and the linear combinations which either minimize (a) or maximize (b) the effect of emission/absorption features are shown in the bottom two panels.

depends on the positioning of the fibre aperture. This is due to a feature of the 2dF corrector lens design which results in relative spatial displacements between different components of a galaxy's spectrum. These displacements can be as large as 1 arcsec (at the 20-arcmin radius) between the incident blue and red components of the observed spectrum. This, together with the previous two uncertainties in placing the fibre aperture, will result in uncertainties in the continuum measurement which make the spectra very difficult to accurately flux-calibrate.

(4) The apparent size of a galaxy on the sky can be larger than the fibre aperture. The positioning of this aperture can therefore result in an unrepresentative spectrum due to spectral gradients within the galaxy.

(5) Atmospheric dispersion (due to imperfect correction) and the differential atmospheric refraction during an exposure each result in errors of the order of <0.3 arcsec.

The source of the chromatic dispersion mentioned above is due to a design feature of the 2dF corrector lens which gives us our extended (2-deg) field of view. This dispersion, combined with the random positioning errors, results in uncertainties in calibrating the continuum of each galaxy spectrum. For this reason we will not make use of the information contained in the continuum of each galaxy in our subsequent analysis. However, we will make use of the continuum calculated by averaging over a sufficiently large ensemble of galaxy spectra, since this will be much more robust (see Section 4.2 for further details).

The random errors in positioning the fibre aperture could also result in uncertainties in measuring the line strengths of emission features such as Hα, since we would expect the strength of this emission to vary spatially across the galaxy. However, because the random positioning errors are much smaller than the scalelengths of the galaxies, this is not a great problem. For this reason the information contained in the emission/absorption line strengths should be relatively robust.

Perhaps our greatest concern regarding the representativeness of the spectra is due to the limited size of the aperture with respect to the galaxy. Surprisingly, we have found it difficult to isolate any systematic bias from this effect. Of course, this effect will be substantially diluted in the observed spectra due to the significant seeing present at the Anglo-Australian Telescope in Siding Springs, which is about 1.5–1.8 arcsec. In addition, the presence of differential atmospheric refraction may also assist us. We discuss the impact of this 'fibre-aperture bias' on our results in more detail in Section 5.3.

3.5 η parametrization

We are presented with several options in attempting to derive a classification for the observed 2dF galaxies based upon their spectra. However, there are several issues that one must first consider.

(1) The distribution of galaxies in the (pc_1, pc_2) plane is smooth (though slightly bimodal), representing a continuous sequence from absorption to emission and from red to blue. There is no evidence to suggest any division into distinct classes of galaxy spectra.

(2) The instrumental errors result in unstable continuum measurements. On the other hand, small-scale features such as line strengths are relatively unaffected.

(3) The relationship between morphology and spectral properties is not very well understood, and hence attempting to anchor the classification using a morphological training set (e.g. Connolly et al. 1995; F99) would be premature. A more robust and quantifiable measure of the galaxy type is required.

By projecting the pc_1 and pc_2 components of each galaxy on to the linear combination which maximizes the effect of emission/absorption line features, we are in effect high-pass filtering the spectra. Thus we would expect (and indeed we find) this projection to be relatively stable to uncertainties in continuum measurements.

By using this projection, we are determining a measure of the average emission/absorption line strength of a galaxy which is easily quantifiable and robust. In addition, this projection is representative of the spectral sequence of the galaxy population, since it is composed of the two most significant principal components (representing 66 per cent of the total variance over the population).

We therefore choose to adopt this projection, which we shall denote by η, as our continuous measure of spectral type

$$\eta = apc_1 - pc_2. \quad (1)$$

The value of a which maximizes the emission/absorption features is essentially identical to that we would find from identifying the most stable projection in the (pc_1, pc_2) plane between repeated pairs of spectral observations. Using this method, we find $a = 0.5 \pm 0.1$.

In Fig. 4 the distribution of the η projections is shown for the galaxies observed to date in the 2dFGRS. Also shown in the same figure is the η–morphology relation for a sample of galaxies from the Kennicutt Atlas (Kennicutt 1992). Comparing the two data sets shows that there is a correspondence between the sequence of η and that of morphology. Note that this correspondence can be treated only as an approximation, since our sample of Kennicutt galaxies is not complete and represents only a few high signal-to-noise ratio spectra with well-determined morphologies. However, the trend is clear.

It is important to have an understanding of the uncertainties in the PCA, as this will affect the reliability of our classification.

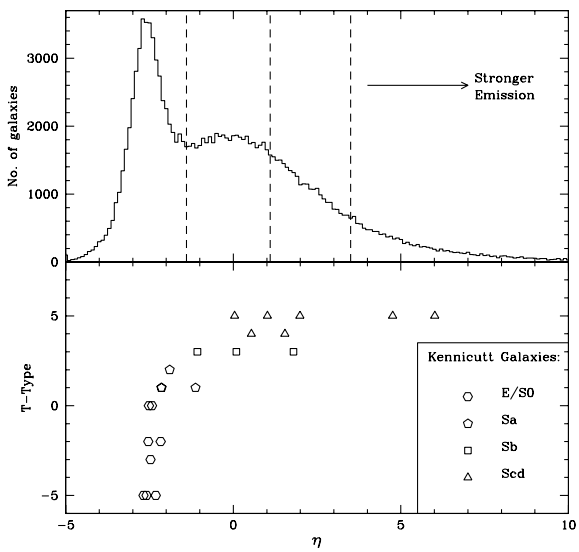

Figure 4. The observed distribution of spectral type measured by η. Also shown are the four divisions we use to divide the dataset (see Fig. 7 for mean spectra). The bottom panel shows the correlation between η and morphological type using a training set of galaxies taken from the Kennicutt Atlas (Kennicutt 1992).

Using a sample of (∼2000) repeated spectral observations, we can attempt to quantify these uncertainties. The differences in the PCA projections (pc_1 and pc_2) and in the spectral classification between repeated pairs is shown in Fig. 5. Note that for clarity we show here the Gaussian fits made to these error distributions. It is clear from this figure that the uncertainty in the pc_1 and pc_2 projections is substantial (1σ dispersions of 2.9 and 1.7 respectively); however, this dispersion is greatly reduced by using the η parametrization ($1\sigma = 0.7$).

In addition to correlating with morphology, η has also been shown to be strongly correlated with the equivalent width of Hα in emission-line galaxies, Fig. 6 (Bland-Hawthorn et al. in preparation). Hence η can be interpreted as a measure of the current star formation present in each galaxy.

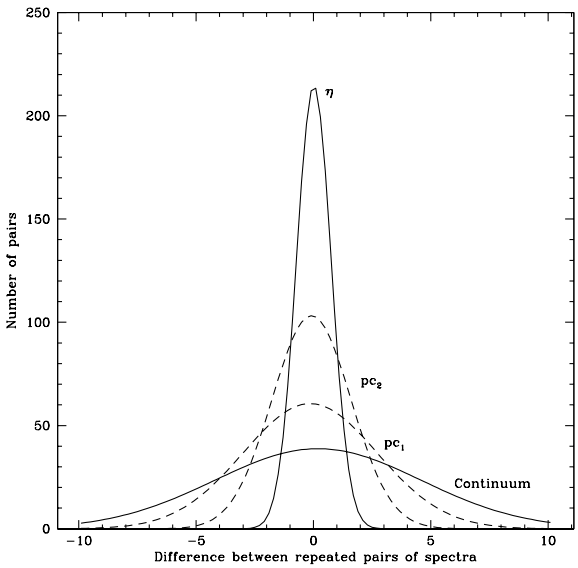

Figure 5. Dispersion in the PCA projections (pc_1 and pc_2) and in the spectral classification η. These distributions are well fitted by Gaussians (shown here), and were calculated by taking the differences in these quantities between ∼2000 repeated spectral observations. Also shown is the dispersion in the orthogonal projection to η, which quantifies the continuum slope in the spectra.

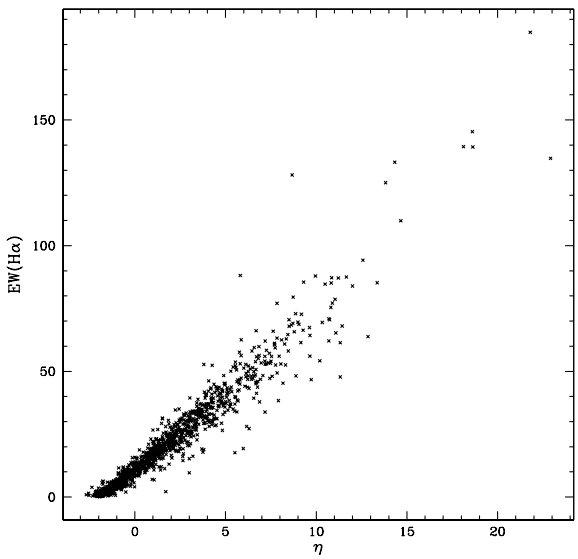

Figure 6. The EW(Hα) is very tightly correlated with η for emission-line galaxies (see Bland-Hawthorn et al. in preparation, for further details).

Note that having a continuous measure of spectral type allows us to take greater advantage of having such a large data set in which much of the detail in the spectral sequence would be smeared out by rough divisions (as in the case of morphological segregation). However, for the purposes of this preliminary analysis we choose to split the spectral sequence into four broad bins ('types') as shown in Fig. 4. The divisions we have made are not determined by the morphological training set (as in previous work), but rather by the shape of the η-distribution itself. The peak in the distribution arises from the degeneracy in spectral line-features between elliptical and early-type spiral galaxies. We separate this peak from the shoulder, which we then divide into two. Another cut is then made to separate the tail of the distribution, which will be dominated by particularly active galaxies such as starbursts and AGNs. The average spectrum of each type is shown in Fig. 7.

4 LUMINOSITY FUNCTIONS

4.1 Completeness

We find that at a depth of $b_J = 19.2$ the density of galaxies is 149.4 deg^{-2} over our targeted area of the sky (Norberg et al. 2001). In order to avoid fibre collisions, it is not possible to assign a fibre to every galaxy in a given field. We take into account this configuration completeness (relative to the parent catalogue) of 93 per cent to calculate the effective area of the observed galaxies, thereby providing the overall normalization for our LF estimates.

In addition to the configuration completeness, it is also necessary to correct for the classification incompleteness: we chose to exclude spectra with $Q < 3$ and signal-to-noise ratio ≤ 10, which do not yield an accurate value of η. We assume that this completeness can be parametrized only in terms of the apparent b_J magnitude, and define

$$C(b_J) = \frac{\text{Galaxies that could be classified}}{\text{Galaxies targeted}}. \quad (2)$$

This ratio is independent of redshift and is appropriate for applications based on conditional probabilities $p(M|z)$, e.g. the STY LF estimator (Section 4.3). In the case of applications where the redshift limits are explicitly set, this completeness ratio is adjusted to take account of this, although this is only a small correction. We find that the classification completeness can be well fitted by a function of the form

$$C(b_J) = \alpha - \exp[\beta(b_J - \gamma)]. \quad (3)$$

We determine the best-fitting parameters by weighting each bin according to the number of galaxies that contributed to it and performing a non-linear least-squares fit, yielding $(\alpha, \beta, \gamma) = (0.96, 1.51, 20.73)$. A weight for each galaxy can then be determined from the inverse of this quantity.

In addition, we note that this parametrization can be significantly skewed in observed fields with low overall completeness. So, before calculating these parameters, we have imposed a minimum completeness threshold for each observed field of 90 per cent. This additional cut reduces the number of galaxies to be used in our calculations by approximately 8000 (as described in Section 2).

The completeness of our sample may also be influenced by other selection biases which vary systematically with redshift or spectral type, e.g. surface brightness. Of course, it is not possible to

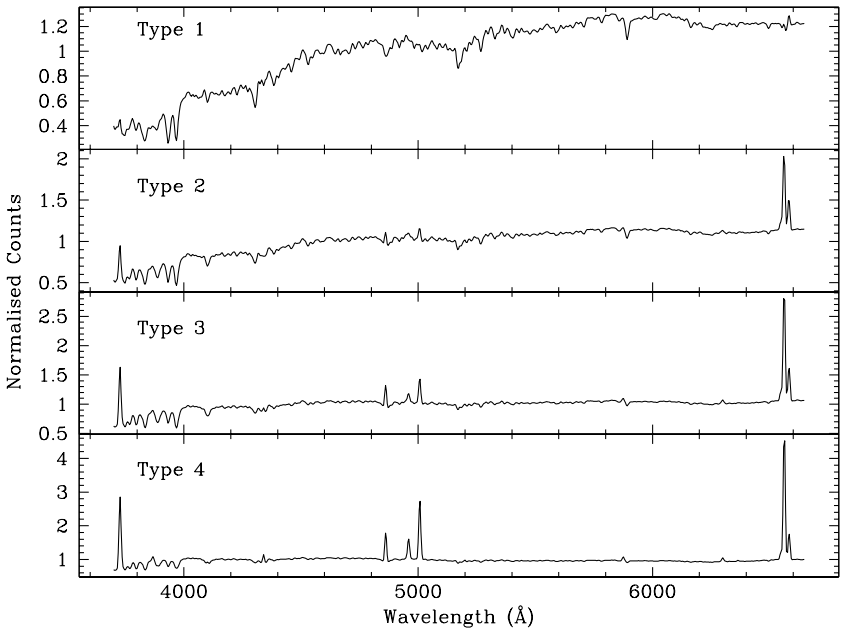

Figure 7. The average 2dFGRS spectrum of each spectral type is shown. Each spectrum is in units of counts per pixel and has been normalized to have average counts of unity.

determine a simple correction for these effects, since we do not know the redshift or spectral type of a galaxy until it has been successfully observed. We expect these additional effects to be small, and they will be discussed in more detail in a forthcoming paper (Cross et al. 2001).

4.2 *k*-corrections

Here we develop a self-consistent method for *k*-corrections based on the observed 2dF spectra. This is a significant improvement compared with previous analyses where the *k*-corrections were anchored to standard SEDs (e.g. Pence 1976) through the relation between morphology and spectral type.

The main obstacle in calculating *k*-corrections directly from the observed spectra is the large uncertainty associated with measuring the continuum (Section 3.4). If this were not an issue, then the calculation of the *k*-corrections would be straightforward, since both the rest frame and observed wavelength range of the 2dFGRS spectra span the range of the b_J passband where the transmission is above 5 per cent of the passband peak (3710–5520 Å).

On a galaxy-by-galaxy basis the continuum uncertainties caused by the chromatic distortion in the telescope optics coupled with the small random fibre positioning errors will induce random errors in the *k*-corrections. We are assisted by the fact that there are only three substantial systematic effects which might affect our calculations:

(i) measuring the b_J passband (Hewett & Warren, private communication);
(ii) determining the 2dF system response (Lewis et al. 2001), and
(iii) aperture bias (Sections 3.4 and 5.3) due to the relatively small size of our fibre aperture compared with the spatial extent of low-redshift galaxies.

Of these three effects, the 2dF system response is by far the least well determined. The system response is calculated using photometric standard star observations with the 2dF instrument set-up, and accounts for the relative photon capturing efficiency of the instrument over different wavelength bands (corrected for seeing). The exact nature of this response is still in the process of being fully determined. For the meantime we adopt a small correction to the previously measured standard-star system response in order to correct the average galaxy survey observation, 1997–2001 (Baldry et al. 2001).

The aperture bias mentioned in the third point can have quite a significant impact on the observed 2dFGRS spectra, since for low-redshift galaxies we will systematically sample more of the (redder) inner bulge light in our spectra. However, this will not lead to significant errors in the absolute luminosities, since at low redshifts, where the aperture bias can be substantial, the *k*-corrections are small in absolute terms; conversely, at higher redshifts, where the *k*-corrections are large, the aperture bias is minimal. We have conducted several tests to estimate the significance of aperture bias on our spectra, and we have found it to be negligible beyond $z \sim 0.1$, particularly due to the relatively poor seeing at the AAT which effectively 'smears' out spectral gradients in each galaxy. In addition, we find that it will have a significant impact only for particularly low-redshift galaxies.

Each individual galaxy spectrum has large uncertainties associated with its continuum, so to calculate meaningful *k*-corrections we adopt here a practical approach. Having divided the galaxies into their respective classes, we proceed to calculate the average spectrum for each class. Since each class contains many thousands of galaxies, it is reasonable to expect any unphysical features present in the spectra to average out (assuming that we have accounted for the above systematic uncertainties). We find from repeated spectral observations that it is equally likely for a continuum to be bent one way as the other, and so, assuming that we have averaged over a sufficient number of galaxy spectra, it is reasonable to assume that these effects will balance out. Therefore each average spectrum can be considered to be a characteristic galaxy template that reflects the true average SED of that ensemble of galaxies. We can now proceed to calculate *k*-corrections for each of these four templates.

Note that we apply these k-corrections to each galaxy individually to calculate its absolute magnitude. However, on a galaxy-by-galaxy basis these derived absolute magnitudes will not be optimal. Rather, they should be interpreted as part of the ensemble to which they belong. We should therefore apply these k-corrections only to applications which involve comparing ensemble properties (e.g., LFs), or alternatively to calculating a property of the entire data set.

We have fitted quadratic forms to the b_J k-corrections given by the following expressions:

$$k_1(z) = 2.6z + 4.3z^2, \quad (4)$$

$$k_2(z) = 1.9z + 2.2z^2, \quad (5)$$

$$k_3(z) = 1.3z + 2.0z^2, \quad (6)$$

$$k_4(z) = 0.9z + 2.3z^2, \quad (7)$$

where k_i refers to the k-correction of type i and is valid over the redshift range $0 < z < 0.2$. The average k-correction over all spectrally classified galaxies is given by $k_{\rm av}(z) = 1.9z + 2.7z^2$. This expression can be used in lieu of the above, or instead could be applied to non-classified galaxies which require k-corrections.

The most substantial source of errors in our k-corrections will arise from the uncertainty in the 2dF system response. Taking this into account, we estimate the uncertainty in our k-corrections to be of the order of 20 per cent.

Norberg et al. (2001) have also calculated k-corrections for the 2dFGRS, independently of the observed galaxy spectra. They find very similar k-corrections, which are consistent with our own to within the stated uncertainty.

4.3 Surface brightness effects

The total b_J magnitudes used in this analysis have been derived from plate scans (Maddox et al. 1990), and so they will be more susceptible to certain systematic effects than those derived from CCD data. In order to improve the accuracy of our magnitudes several recalibrations of the b_J magnitudes have been made using CCD photometry from overlapping fields (see Norberg et al. 2001).

Unfortunately, some small offsets still remain. One such effect which may be important to the analysis of LFs per spectral type is an apparent shift in b_J magnitude with surface brightness (Cross 2001; Blanton et al. private communication). Fig. 8 shows the offsets between the 2dFGRS b_J magnitudes and those derived from a CCD photometric survey (Cross 2001; Cross et al. in preparation) versus surface brightness; a trend is clear in that high surface brightness objects tend to be systematically fainter in 2dFGRS b_J. These offsets are most likely due to a saturation effect in the (plate derived) 2dFGRS magnitudes.

These small offsets will have a negligible effect on the calculation of the overall LF, but may be significant when one divides the 2dFGRS sample in a way which is related to surface brightness. Fig. 9 shows how these shifts depend upon our spectral classification; it can be seen that the relationship is surprisingly weak.

The mean shifts we calculate per type are, however, significant compared to their estimated uncertainties (Table 2), particularly for the most late-type galaxies. We correct the galaxy magnitudes for each spectral type in order to account for these shifts in the analysis that follows.

4.4 Estimators

We assume a flat homogeneous universe with a uniform Hubble

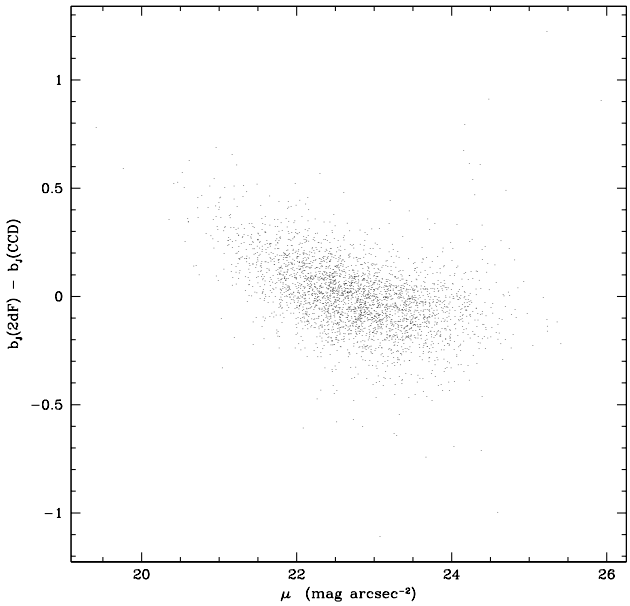

Figure 8. The shift between the 2dFGRS b_J magnitude and that derived from a CCD photometric survey (Cross et al. in preparation) is shown for $\sim$3000 galaxies. It can be seen that the shift varies systematically with surface brightness, and so care must be taken when dividing the sample.

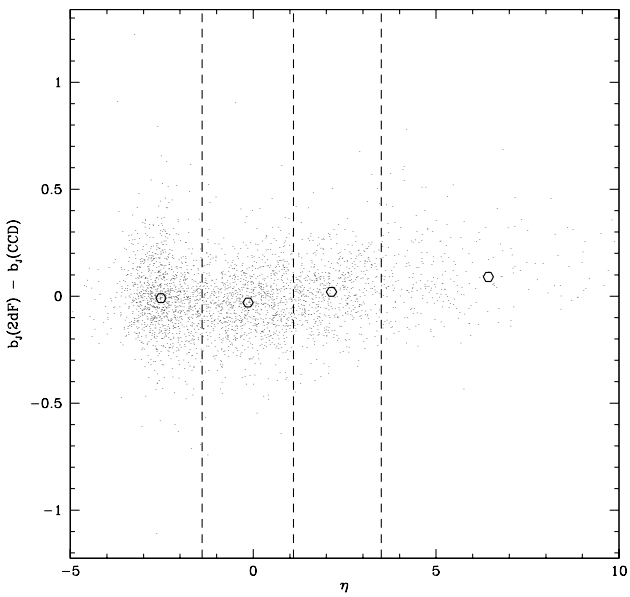

Figure 9. The b_J magnitude error versus spectral type (η) is shown. It can be seen that there is a weak correlation between the two quantities.

Table 2. The mean shifts between the 2dFGRS b_J magnitudes and the CCD magnitudes per spectral type. The stated uncertainties are 1σ.

Type	Mean shift (mag)	Uncertainty
1	−0.009	0.005
2	−0.033	0.004
3	0.024	0.006
4	0.09	0.01

flow ($h = H_0/100\,\mathrm{km\,s^{-1}\,Mpc^{-1}}$), a cosmological constant $\Omega_\Lambda = 0.7$, and a mass density parameter $\Omega_\mathrm{m} = 0.3$. In computing the LFs we use both the step-wise maximum-likelihood (SWML) method (EEP88) to make a non-parametric fit to the LF, and the STY method (Sandage, Tammann & Yahil 1979) to calculate the maximum-likelihood Schechter function fit to the LF,

$$\phi(L)\,\mathrm{d}L = \phi^* \left(\frac{L}{L^*}\right)^{\alpha} \exp\left(-\frac{L}{L^*}\right)\frac{\mathrm{d}L}{L^*}. \tag{8}$$

Both of these estimators are discussed extensively in the literature (e.g. EEP88; Willmer 1997). In addition, we take into account the presence of Malmquist bias in our STY fit by assuming that the errors in the b_J magnitudes are Gaussian ($\sigma_M = 0.15$; see Colless et al. 2001). The observed LF will then be a convolution of the true LF with the distribution of magnitude errors,

$$\phi_\mathrm{obs}(M) = \frac{1}{\sqrt{2\pi}\sigma_M}\int_{-\infty}^{\infty} \phi(M')\,\mathrm{e}^{-(M'-M)^2/2\sigma_M^2}\,\mathrm{d}M'. \tag{9}$$

Neither method predicts the normalization of the LF, so we estimate this independently by fitting to the projected counts,

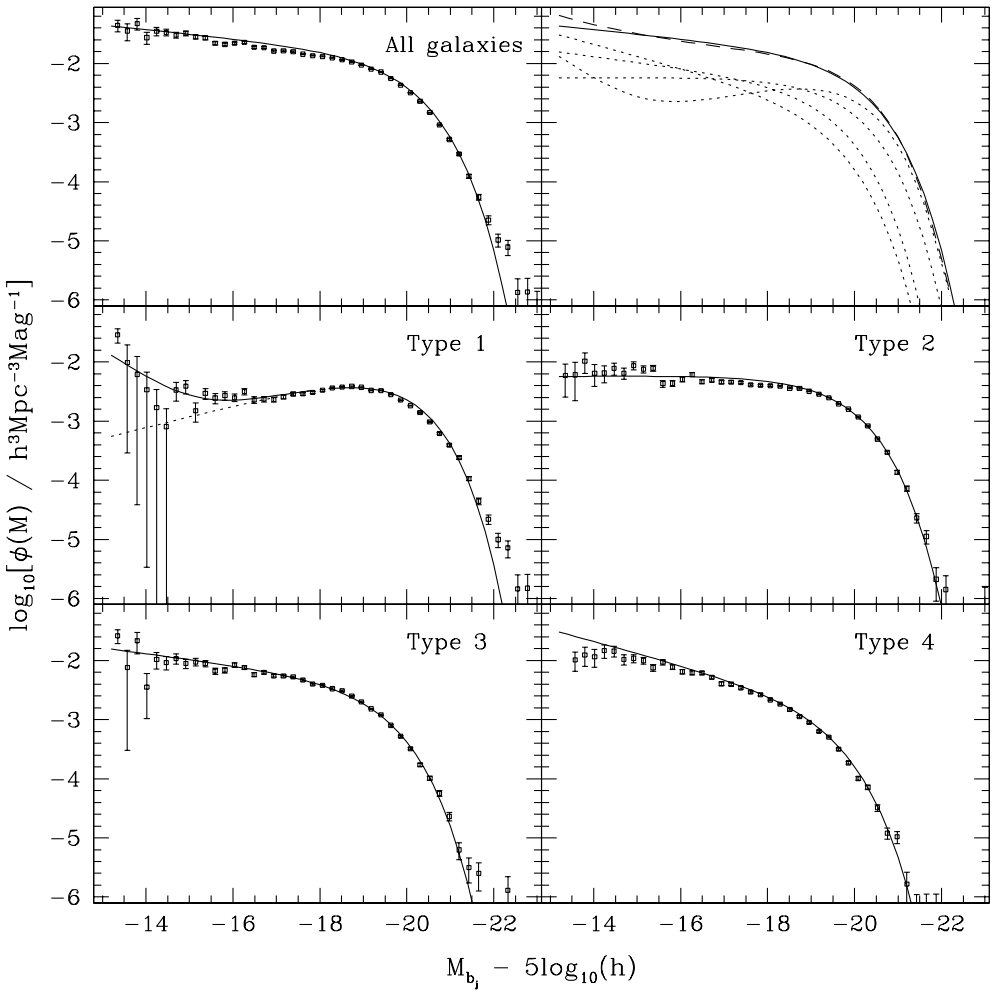

Figure 10. The luminosity functions derived per spectral type. The top left box shows the LF derived from all the classified galaxies, and the top right box shows how this (solid line) relates to the summation of the fitted LFs per type (dashed line). For each of the remaining four panels we show the SWML points and Schechter fits to the LF per spectral type. The Schechter function has been fitted over the entire range in M_{b_J} magnitude for Types 2, 3 and 4, and only out to $M_\mathrm{lim} - 5\log_{10}(h) = -17$ for Type 1. For Type 1 we show the best-fitting Schechter function for the bright galaxies (dotted line) and the combination of this with our analytic form for the faint-end residuals (solid line). Our assumed cosmology here is $\Omega_\mathrm{m} = 0.3$, $\Omega_\Lambda = 0.7$.

Table 3. Schechter function parameters derived in our analysis per spectral type using galaxies with $M_{b_\mathrm{J}} < M_\mathrm{lim}$. The errors given are $\pm 1\sigma$. The normalization, ϕ^*, of the Schechter function is in units of $10^{-3}\,h^3\,\mathrm{Mpc}^{-3}$, and $\rho_L = \phi^* L^* \Gamma(\alpha+2)$ is the luminosity density in units of $10^7\,\mathrm{L}_\odot\,h\,\mathrm{Mpc}^{-3}$ ($M_{b_\mathrm{J}\odot} = 5.30$).

Sample	η	$M_\mathrm{lim} - 5\log_{10}(h)$	# Galaxies	$M^* - 5\log_{10}(h)$	α	ϕ^*	ρ_L
All	–	−13.0	75589	−19.79 ± 0.04	−1.19 ± 0.01	15.9 ± 1.0	19.9 ± 1.4
1	$\eta < -1.4$	−17.0	27540	−19.58 ± 0.05	−0.54 ± 0.02	9.9 ± 0.5	7.8 ± 0.5
2	$-1.4 \le \eta < 1.1$	−13.0	24256	−19.53 ± 0.03	−0.99 ± 0.01	7.2 ± 0.4	6.1 ± 0.4
3	$1.1 \le \eta < 3.5$	−13.0	15016	−19.17 ± 0.04	−1.24 ± 0.02	5.0 ± 0.3	3.7 ± 0.3
4	$\eta \ge 3.5$	−13.0	8386	−19.15 ± 0.05	−1.50 ± 0.03	2.4 ± 0.2	2.6 ± 0.3

$149.4\,\mathrm{deg}^{-2}$ (Section 4.1). In so doing, we make the assumption that the type fractions in the parent catalogue are identical to those of the classified galaxies (over the redshift interval $0.01 \leq z \leq 0.15$).

5 DISCUSSION

5.1 Results

Having performed the calculations outlined above (see Fig. 10 and Table 3), we find that the Schechter function provides an inadequate fit of the LF calculated over the entire range in M_{b_J} magnitude, especially for our most passive and active star-forming galaxies (Types 1 and 4 respectively). In order to determine a better fit to the LF of the passive (Type 1) galaxies, we have applied the following simple procedure. First, we fitted a Schechter function to the LF of the bright galaxies [$M_{b_J} - 5\log_{10}(h) < -17$] using the STY method. This provides an adequate representation of the data over the brightest ranges in magnitude. Having calculated this fit, we then found that the residual LF at the faint end could be well fitted by a function of the form

$$\phi_{\mathrm{res}}(M_{b_J}) = 10^{(a+bM_{b_J})}, \tag{10}$$

particularly for the magnitude range $-17 < M_{b_J} - 5\log_{10}(h) < -14.5$ where the error bars are small. We calculated a and b using a least-squares fit to the residual created by subtracting the STY fit from the SWML points at the faint end. The LF at the faint end can then be described by the combination

$$\phi(M) = \phi_{\mathrm{Sch}}(M; \alpha, M^*, \phi^*) + \phi_{\mathrm{res}}(M; a, b), \tag{11}$$

where $(a, b) = (4.7, 0.50)$. The uncertainties in these parameters are quite large (± 0.9, ± 0.06), an obvious consequence of the large errors in the SWML points at these magnitudes.

We estimate the scatter in our derived Schechter parameters by performing a large number of random realizations drawn from the estimated LFs. In addition to this sampling variance, we also take into account the uncertainties in our k-corrections (20 per cent) and in the number density of the galaxies (7 per cent). The quoted errors are at the 1σ level.

The two most notable features of our derived LFs are the systematic variation of the faint-end slope (α) and the characteristic magnitude (M^*) with spectral type. The faint-end slope steepens significantly from $\alpha = -0.54$ for the most passive star-forming galaxies (Type 1) to $\alpha = -1.50$ for the most active galaxies (Type 4). On the other hand, the characteristic magnitude becomes systematically fainter as we go from the most passive [$M^* - 5\log_{10}(h) = -19.58$] to active [$M^* - 5\log_{10}(h) = -19.15$] star-forming galaxies. These results agree with previous measurements in that the late-type galaxies are systematically fainter than their early-type counterparts.

Note that our results do not change much if we exclude our correction for the errors in our b_J magnitudes ($\Delta M^* = 0.05$–0.06, $\Delta\alpha = 0.02$–0.05).

The fact that the Schechter function is not a good fit to the data over the entire M_{b_J} magnitude range is mostly due to an over- (Type 1) or under- (Type 4) abundance of faint objects relative to bright objects. This is particularly true of the passive (Type 1) sample of galaxies, for which there is a very significant increase in the predicted number density of faint galaxies. This feature has been present in previous analyses (e.g. F99); however, the small sample size has meant that only a statistically insignificant number of galaxies have contributed. Hence previous studies could not determine if this feature was real or a consequence of the small volume being sampled at these magnitudes. For the first time here we show significant evidence for the presence of a substantial dwarf (passive star-forming) population with 142 galaxies having $M_{b_J} - 5\log_{10}(h)$ magnitude fainter than -16.0 ($\bar{z} = 0.027$). Of course, these objects will tend to have low signal-to-noise ratio spectra, so some degree of contamination in this sample should be present, particularly from erroneous redshift determinations. However, these preliminary results look promising, and we expect more detailed analyses to be forthcoming in the near future.

5.2 Previous results

F99 has performed similar calculations of the LF per spectral type using a subset of the data presented here. In Fig. 11 we compare their results with those presented here. Note that in order to make this comparison we have recalculated the LFs assuming (for consistency) an Einstein–de Sitter universe ($\Omega = 1$, $\Lambda = 0$), and we have reduced the five classes of F99 to our four types by taking linear combinations of their LFs which give the same fractions of galaxies per type as our own. It can be seen from the figure that our results are in good agreement with those of F99, except for some small systematic shifts. These differences are due to four factors which we believe have significantly improved the accuracy of our analysis.

(i) We have used a considerably larger sample of galaxies in our calculations.

(ii) We have adopted self-consistent k-corrections, resulting in a small change in the predicted M^* and ϕ^*.

(iii) Taking into account recent advances in our CCD calibrations, we have been able to update the catalogue b_J

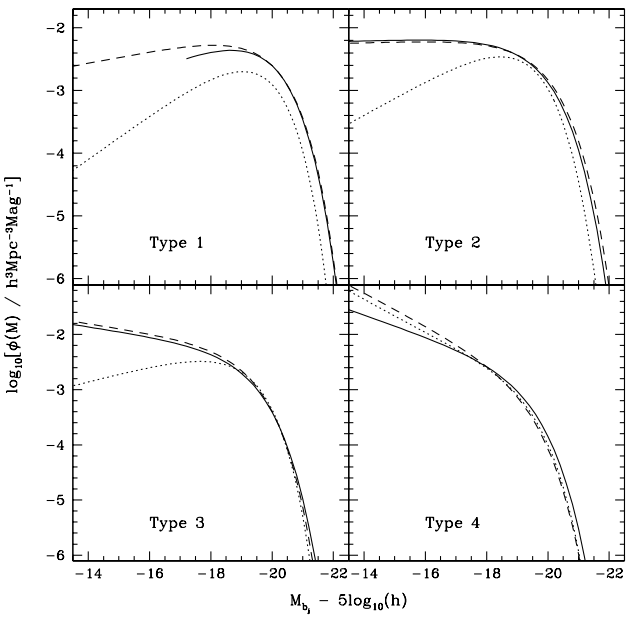

Figure 11. Comparison with the type-dependent LFs calculated by Folkes et al. (dashed lines) and Bromley et al. (dotted lines). The solid lines show our LFs assuming (for consistency) an Einstein–de-Sitter Universe. Note that the Type 1 LF has only been fitted to $M_{b_J} - 5\log_{10}(h) < -17$. The disagreement between the different sets of determinations may be due to the poor fit of the Schechter function to the LF, or to different selection effects between the surveys.

magnitudes (Colless et al. 2001; Norberg et al. 2001). This has also resulted in a small change in the number counts and hence ϕ^*.

(iv) We have corrected for saturation effects in high surface brightness objects (Section 4.3). This has a particularly large impact on our most late-type (Type 4) galaxies.

The most similar independent analysis of the LF per spectral type has been conducted by Bromley et al. (1998), using the Las Campanas Redshift Survey. We also compare these results with our own in Fig. 11. Again, in order to compare the six clans with our four types, we have had to combine their LF determinations in a way which yields the same fractions of galaxies per type as our own. In addition, we have applied the transformation $M_{b_J} = M_r + 1.1$ (Lin et al. 1996) to convert the LCRS Gunn-r magnitudes to b_J.

The trend of the galaxy LFs to become progressively fainter as one moves from passive to active star-forming galaxies is clear for both sets of results. However, there appears to be some significant disagreement, particularly in the faint-end slope between the two LF determinations. Given the poor fit of the Schechter function to the faint end of the LF, we would not expect these two sets of results to necessarily agree within their stated errors. The large differences observed are most probably due to the different selection effects (e.g., surface brightness and b_J versus r selection) which can be particularly prominent for fainter galaxies, hence adding more uncertainty to α than can be estimated from a standard error analysis.

Our total luminosity density (again assuming an Einstein–de-Sitter Universe) is within 4 per cent of the figure obtained in F99, and is 30 per cent lower than the figure quoted by Blanton et al. (2001) for the Sloan Digital Sky Survey early data release. The reasons for this discrepancy are discussed in Norberg et al. (2001), but in summary we believe that the Blanton et al. figure is too high, partly owing to large-scale structure in their small initial sample, and also through the use of an inappropriate colour equation to predict 2dFGRS magnitudes.

5.3 Aperture effects and evolution

The spectra observed as part of the 2dFGRS are acquired through optical fibres with a diameter of 140 μm, corresponding to between 2 and 2.16 arcsec on the sky (depending on plate-position; see Lewis et al. 2001). In our assumed cosmology ($\Omega_m = 0.3$, $\Omega_\Lambda = 0.7$) this translates to an aperture width of approximately $2.8\,h^{-1}$ kpc at the survey median redshift of $z = 0.1$. The fact that fitted galaxy brightness profiles have scalelengths of the order of 3–4 kpc (Binney & Merrifield 1998) raises the question of how representative the observed spectra are of the galaxies as a whole. However, with typical seeing (1.5′–1.8 arcsec) and random fibre positioning errors (rms 0.3 arcsec) the 2dF fibre-aperture will in fact sample a much larger portion of each galaxy.

If the effective fibre apertures were significantly smaller than the galaxies over a range of redshifts, then the variation in this aperture with redshift would result in systematic biases in the determination of the LFs. These so-called 'aperture effects' are difficult to quantify without an in-depth knowledge of the spatially resolved spectral properties of the targetted galaxies.

Kochanek, Pahre & Falco (2000) recently suggested a test to estimate the influence of this fibre-aperture bias on the determination of type-dependent LFs $\phi_i(M)$. The test involves comparing the observed fractional number counts of galaxies in each class to the fractional number counts predicted by our derived LFs. Kochanek et al. found that for redshift surveys classified morphologically the two were generally consistent, but that for surveys classified spectrally using fibre-aperture spectra the two were very inconsistent. We have performed this test on our data, and found no substantial inconsistencies (Fig. 12). With the exception of small systematic offsets, the observed type fractions were found to agree with those predicted by the LF to within 2σ over the entire range in b_J magnitude. We note that as the number counts predicted by the LF are normalized by construction to the observed number counts, this test is only necessary and not sufficient. For this reason more sophisticated tests such as

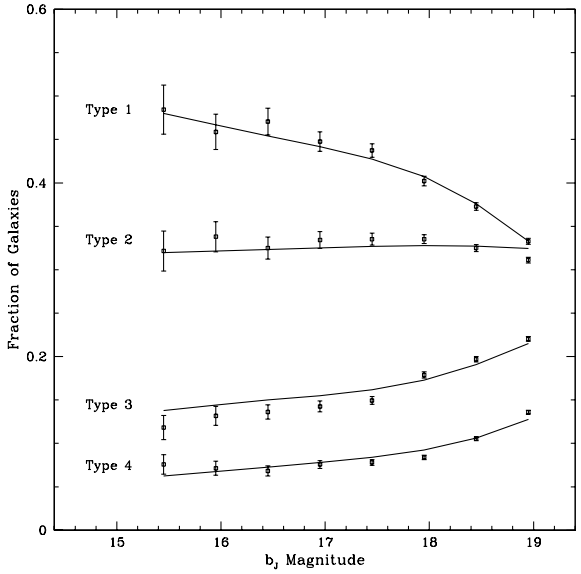

Figure 12. A test recently proposed by Kochanek et al. (2000). We show observed (squares) and predicted (lines) type fractions for the 2dF galaxies used in our calculations, where the predicted fractions have been derived from integrating our LFs. The two are consistent within the stated (Poisson) errors.

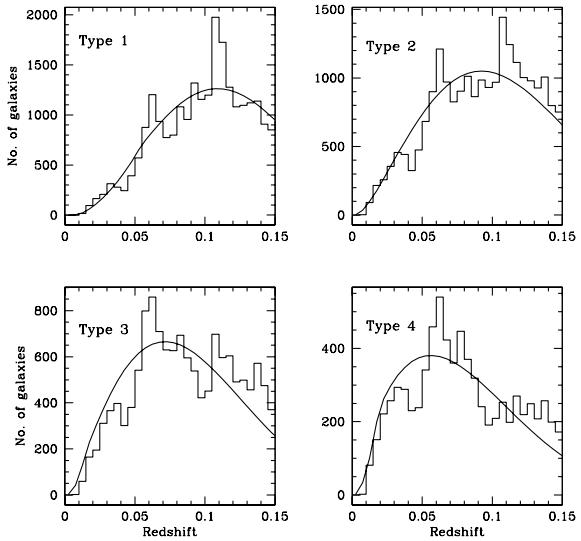

Figure 13. Comparison between the observed $N(z)$ distributions (histograms) and the predicted $N(z)$ for each spectral type ($b_J < 19.3$). Note that the $N(z)$ distributions of the first two types are recovered very well, but that significant deviations exist for the last two (most active star-forming) types.

comparisons with detailed models are necessary in order to isolate and analyse the competing effects on the data (e.g., positional errors, seeing and evolution).

We show the observed and predicted $N(z)$ distributions for each spectral type out to $b_J < 19.3$ in Fig. 13. It can be seen that the observed $N(z)$ is well recovered by the LF for the first two types. There appears to be a significant over abundance of high-z galaxies for the two highest star-forming types, as well as a slight under abundance of low-z galaxies. Similar deviations in abundance could be explained by aperture effects. However, if this were the only explanation, then we would also observe a significant over abundance of low-z passive star-forming galaxies, which is not the case. A much more reasonable explanation for these deviations between the predicted and observed $N(z)$ distributions is the presence of evolution (see, e.g., Lin et al. 1999). Because these two effects affect the observed galaxy population in similar ways, they will be difficult to disentangle in more detailed analyses. For the present, we note that as far as the determination of the LF in broad bins of spectral type is concerned, both of these biases have only a small effect on our calculations.

6 CONCLUSIONS

In this paper we have applied a method of spectral classification, η, based on the relative emission/absorption line strength present in a galaxy's optical spectrum. This classification correlates well with morphology, and we interpret it as a measure of the relative current star formation present in each galaxy. Based on this classification, we have divided the galaxies observed to date in the 2dFGRS into four spectral types, and calculated the LF for each. Our results are consistent with previous determinations in that the faint-end slope systematically steepens, and the characteristic magnitude becomes fainter as we move from passive to active star-forming galaxies. In addition, we have been able to show that the Schechter function is a poor fit to the LF over a large range of M_{b_J} magnitudes, perhaps as a result of subpopulations within the data. The calculations presented in this letter represent the most accurate determinations of the optical b_J galaxy LF to date.

As η is a continuous variable, the next step in quantifying the variation of the LF with spectral type is to develop a bivariate formalism $\phi(M,\eta)$. Such a result would be extremely valuable in that it would quantify the variation in the Schechter parameters with galaxy type, $\alpha(\eta)$ and $M^*(\eta)$, allowing the results to be applied much more objectively to such things as semi-analytic models from which spectra as well as other galaxy properties can be derived (e.g. Slonim et al. 2001, and references therein). We can then also extend this approach of comparing the observed LFs with model LFs by mimicking the observational selection effects (e.g., aperture bias).

One of the key advantages of our spectral type, η, is that it can easily be applied to any other set of galaxy spectra which occupy the relevant wavelength range. This will be invaluable when comparing results from the many different galaxy surveys currently underway (e.g., SDSS, VIRMOS, 6dF, etc.).

The 2dF Galaxy Redshift Survey has made available to the community 100 000 galaxy spectra and redshifts through their website, `http://www.mso.anu.edu.au/2dFGRS/`. Additional information regarding the spectral classification and LFs presented here can be obtained from `http://www.ast.cam.ac.uk/~twodfgrs/`.

ACKNOWLEDGMENTS

DSM was supported by an Isaac Newton Studentship from the University of Cambridge and Trinity College. We thank R. Kaldare, S. Ronen and R. Somerville for many helpful discussions. The 2dF Galaxy Redshift Survey was made possible through the dedicated efforts of the staff at the Anglo-Australian Observatory, both in creating the two-degree field instrument and supporting it on the telescope.

REFERENCES

Baldry I. K. et al. (the 2dFGRS Team), 2001, ApJ, accepted (astro-ph/0110676)
Binney J., Merrifield M., 1998, Galactic Astronomy. Princeton Univ. Press, Princeton
Blanton M. et al. (the SDSS Collaboration), 2001, AJ, 121, 2358
Bromley B. C., Press W. H., Lin H., Kirshner R. P., 1998, ApJ, 505, 25
Colless M. M. et al. (the 2dFGRS Team), 2001, MNRAS, 328, 1039
Connolly A. J., Szalay A. S., Bershady M. A., Kinney A. L., Calzetti D., 1995, AJ, 110, 1071
Cross N. J. G., 2001, PhD thesis, Univ. St Andrews
Cross N. J. G. et al. (the 2dFGRS Team), 2001, MNRAS, 324, 825
Efstathiou G., Ellis R. S., Peterson B. A., 1988, MNRAS, 232, 431 (EEP98)
Ellis R. S., Colless M., Broadhurst T., Heyl J., Glazebrook K., 1996, MNRAS, 280, 235
Folkes S. R., Lahav O., Maddox S. J., 1996, MNRAS, 283, 651
Folkes S. et al. (the 2dFGRS Team), 1999, MNRAS, 308, 459 (F99)
Glazebrook K., Offer A. R., Deeley K., 1998, ApJ, 492, 98
Heavens A. F., Jimenez R., Lahav O., 2000, MNRAS, 317, 965
Kennicutt R. C., Jr, 1992, ApJS, 79, 255
Kochanek C. S., Pahre M. A., Falco E. E., 2000, ApJ, submitted (astro-ph/0011458)
Lahav O., 2000, to appear in 'ESO Astrophysics Symposia'. Springer-Verlag (astro-ph/0012407)
Lewis I. et al., 2001, MNRAS, accepted
Lin H., Kirshner R. P., Schectman S. A., Landy S. D., Oemler A., Tucker D., Schechter P. L., 1996, ApJ, 464, 60
Lin H., Yee H. K. C., Carlberg R. G., Morris S. L., Sawicki M., Patton D. R., Wirth G., Shepherd C. W., 1999, ApJ, 518, 533
Loveday J., Tresse L., Maddox S., 1999, MNRAS, 310, 281
Maddox S. J., Efstathiou G., Sutherland W. J., 1990, MNRAS, 246, 433
Marzke R. O., da Costa L. N., 1997, AJ, 113, 185
Norberg P. et al., 2001, MNRAS, submitted (astro-ph/0111011)
Pence W., 1976, ApJ, 203, 39
Ronen S., Aragón-Salamanca A., Lahav O., 1999, MNRAS, 303, 197
Sandage A., Tammann G. A., Yahil A., 1979, ApJ, 232, 352
Slonim N., Somerville R., Tishby N., Lahav O., 2001, MNRAS, 323, 270
Wilmer C. N. A., 1997, AJ, 114, 898

This paper has been typeset from a TEX/LATEX file prepared by the author.